Are urban material gradients transferable between areas?

Chaonan Ji[a,b,*], Uta Heiden[c], Tobia Lakes[a,d], Hannes Feilhauer[e]

[a]*Applied Geoinformation Science lab, Geography Department, Humboldt Universität zu Berlin, Unter den Linden 6, 10099 Berlin, Germany*
[b]*German Remote Sensing Data Center (DFD), German Aerospace Center (DLR), Oberpfaffenhofen, 82234 Wessling, Germany*
[c]*Remote Sensing Technology Institute (IMF), German Aerospace Center (DLR), Oberpfaffenhofen, 82234 Wessling, Germany*
[d]*Integrative Research Institute on Transformations of Human-Environment Systems (IRI THESys), Humboldt Universität zu Berlin, Unter den Linden 6, 10099 Berlin, Germany*
[e]*Remote Sensing Centre for Earth System Research, Universität Leipzig, Talstr. 35, 04103 Leipzig, Germany*

Abstract

Urban areas contain a complex mixture of surface materials resulting in mixed pixels that are challenging to handle with conventional mapping approaches. In particular, for spaceborne hyperspectral images (HSIs) with sufficient spectral resolution to differentiate urban surface materials, the spatial resolution of 30 m (e.g., EnMAP HSIs) makes it difficult to find the spectrally pure pixels required for detailed mapping of urban surface materials. Gradient analysis, which is commonly used in ecology to map natural vegetation consisting of a complex mixture of species, is therefore a promising and practical tool for pattern recognition of urban surface material mixtures. However, the gradients are determined in a data-driven manner, so analysis of their spatial transferability is urgently required. We selected two areas—the Ostbahnhof (Ost) area and the Nymphenburg (Nym) area in Munich, Germany—with simulated EnMAP HSIs and material maps, treating the Ost area as the target area and the Nym area as the well-known area. Three gradient analysis approaches were subsequently proposed for pattern recognition in the Ost area for the cases of (i) sufficient samples collected in the Ost area; (ii) some samples in the Ost area; and (iii) no samples in the Ost area. The Ost samples were used to generate an ordination space in case (i), while the Nym samples were used to create the ordination space to support the pattern recognition of the Ost area in cases (ii) and (iii). The Mantel statistical results show that the sample distributions in the two ordination spaces are similar, with high confidence (the Mantel statistics are 0.995 and 0.990, with a significance of 0.001 in 999 free permutations of the Ost and Nym samples). The results of the partial least square regression models and 10-fold cross-validation show a strong relationship (the calculation-validation R^2 values on the first gradient among the three approaches are 0.898, 0.892; 0.760, 0.743; and 0.860, 0.836, and those on the second gradient are 0.433, 0.351; 0.698, 0.648; and 0.736, 0.646) between the ordination scores of the samples and their reflectance values. The mapping results of the Ost area from three approaches also show similar patterns (e.g., the distribution of vegetation, artificial materials, water, ceremony area) and characteristics of urban structures (the intensity of buildings). Therefore, our findings can help assess the transferability of urban material gradients between similar urban areas.

Keywords: hyperspectral image, urban mapping, gradient analysis, transferability, imaging spectroscopy

1. Introduction

The majority of the world population lives in urban areas, and the number of urban residents is increasing as more regions are rapidly becoming urbanized (DESA, 2018). Accurate and up-to-date maps are important for modelers to study meteorology (Auer Jr, 1978), climatology (Seto and Shepherd, 2009), and ecology (Lakes and Kim, 2012) and for local authorities to understand the growth dynamics and rapid spatial development of their cities (Cao et al., 2020). However, detailed mapping of urban surfaces is challenging because urban surface materials feature complex spatial patterns, i.e., spatially and spectrally heterogeneous natural and artificial land covers (Chen et al., 2018).

Hyperspectral remote sensing has become an important tool in Earth observation. It extends the number of spectral bands from several or dozens to hundreds, providing a continuous spectrum to identify the materi-

*Corresponding author
Email address: ji.chaonan@dlr.de (Chaonan Ji)

als based on their specific reflectance features (Herold et al., 2004; Heiden et al., 2007). Hyperspectral images (HSIs) that contain a considerable amount of detailed information on land cover and the state of the environment can be used for various applications such as urban modelling (van der Linden et al., 2019), ecological surveys (Degerickx et al., 2018; Skowronek et al., 2018), and geological analyses (Kruse et al., 2003). Spaceborne HSIs can provide global coverage with high temporal resolution to support operational product generation and commercial exploitation of the data, for example, to support economic growth as planned for the Copernicus CHIME mission (Nieke and Rast, 2019) and to support climate-related research, which is one of the goals of NASA's SBG mission (Lee et al., 2015) and the upcoming German EnMAP mission (Guanter et al., 2015). The currently operating missions, such as the Italian PRISMA mission (Loizzo et al., 2019) and the German/US mission DESIS (Alonso et al., 2019), are already delivering data on an operational basis for the development of techniques and scientific data products.

However, the acquisition of spaceborne HSIs with sufficient spectral and spatial resolution, good signal-to-noise ratios (SNRs) and high revisit times is still challenging. Due to sensor design considerations, the rich spectral information in hyperspectral data is often not complemented by extremely fine spatial resolution (Li et al., 2012). For HSIs with 30 m $\times$ 30 m spatial resolution (e.g., recorded by EnMAP), a large number of surface materials on the measurement scale can be mixed. The resulting mixed pixels reflect the composite spectral response of the contained materials, so the application of per-pixel classifiers to images dominated by mixed pixels may result in inaccurate classification (Plaza et al., 2009).

Gradient analysis appears to be a promising approach for addressing the problem of mixed pixels. Gradient analysis is commonly used in ecology to describe and map natural vegetation by treating all pixels as mixed and to describe and quantify the gradual transitions in the cover fractions of the different species (Schmidtlein and Sassin, 2004; Feilhauer et al., 2011, 2014, 2020; Neumann et al., 2016; Neumann, 2017). Urban environments contain districts with similar structural and compositional characteristics and thus display the co-occurrences of certain urban surface materials. For example, industrial areas often consist of large low- to medium-rise buildings and predominantly impervious open surfaces, whereas residential areas such as detached housing settlements are likely composed of small low-rise buildings and pervious surfaces such as lawns, meadows and trees (Heldens, 2010). When applying the gradient concept to an urban area, urban material gradients were proposed, and it was then confirmed that such gradients exist in urban space and can be linked to spectral mixtures (Jilge et al., 2019).

However, gradients are generally determined in a data-driven manner. Hence, gradients may be only locally suitable so that additional field data collection will be required, if the gradients are transferred to other unknown areas. Such data collection can be a expensive and time-consuming task. Consequently, an analysis and assessment of the transferability of gradients is crucial for their broader application. As a first step in this direction, Ji et al. (2020) analysed the sampling robustness of gradient analysis with slight movement of the sampling location and different sampling schemes. The influence of such slight movements was marginal, and therefore, the next step will be to study the transferability of urban material gradients to unknown areas.

Therefore, the objective of this study is to analyse the area transferability of urban material gradients over two subsets of Munich, Germany. We aim to address the following two questions: (i) Are the urban material gradients transferable between the two study sites? (ii) What affects the transferability of urban material gradients? Our results will provide insights regarding the general feasibility of gradient transfer to urban areas, where there is either limited or no information regarding the surface material compositions. As a first step to addressing this problem, we have chosen two areas in Munich, Germany, that are composed of similar urban neighborhoods with expected similar surface material compositions. Based on the findings, we discuss the potential applications of the transferable urban gradients.

2. Study area and data

2.1. Study site

The present study was conducted on two subsets of Munich, Germany (Fig. 1). The first is located in the south-east of Munich city (48.106°N to 48.133°N, 11.565°E to 11.632°E) and is referred to as the Ostbahnhof (Ost) area in this study because it covers the Munich east train station. The Ost area is considered a perfect urban study area because it consists of complex and typical German urban structures (Heiden et al., 2012), i.e. it represents an inner-city, densely built-up area with residential and commercial buildings from different epochs. The second study area covers the Nymphenburg Palace and is hence called the Nymphenburg (Nym) area; by contrast, this area is characterized

by larger vegetation-covered areas (e.g., Nymphenburg Palace Park, Hirschgarten, and Olympia Park). The Nym area was chosen for the transferability analysis of urban gradients because, on the one hand, it has material classes similar to those of the Ost area, while, on the other hand, it contains a unique set of materials in the palace area.

2.2. Simulated EnMAP HSIs

The simulated EnMAP HSIs are modelled from the HyMap data acquired by the German Aerospace Center in June 2007 during the HyEurope mission. The HyMap data cover the Ost and Nym areas with two north-south-oriented flight lines. The HyMap imagery includes 128 spectral bands in the range from 450 *nm* to 2500 *nm* with a ground sampling distance (GSD) of 4 m. The data were pre-processed and are reported with an average root mean square error (RMSE) of 0.8 pixels (Heldens, 2010; Heiden et al., 2012). The simulated EnMAP images are characterized by a GSD of 30 m and 242 bands ranging from 423 *nm* to 2439 *nm* (Segl et al., 2012; Guanter et al., 2015). The SWIR data of the EnMAP imagery were taken into account in the overlapping of the VNIR and SWIR sensors. Additional spectral bands ranging from 1358 *nm* to 1418 *nm* and 1814 *nm* to 1951 *nm* were eliminated due to atmospheric water absorption. Therefore, 210 bands of simulated EnMAP HSIs were used in this study.

2.3. Material map

The material maps of these two subsets were obtained from a previous study of HyMap HSIs by Heldens (2010). The Ost material map was pre-processed by Jilge et al. (2019) omitting the invalid materials (e.g. shadow, unclassified pixels) that play minor and or no roles in the study area, and thus, 27 material classes were considered. Correspondingly, three additional material classes (lake, pool, coniferous tree) included in the Nym area were omitted because the transferability approach requires the same material classes among different study areas.

3. Methods

To test the transferability of the urban gradients, we systematically defined three different conditions, developed the corresponding approaches, and compared the findings for the derived model outcomes and prediction maps. The three conditions were as follows: (i) sufficient Ost samples to produce urban material gradients; (ii) some Ost samples but not enough to perform a gradient analysis; (iii) no Ost samples and therefore no possibility of extraction of the local gradients. We sought to interpret the Ost area under these three conditions, with the assumption that the Nym area provides sufficient samples to generate the urban material gradients. Based on these assumptions, three gradient analysis approaches were constructed as shown in Fig. 2. The first approach was used as the control approach (approach-OstOst), and the other approaches are experimental approaches (approach-OstNym and approach-NymNym).

All analyses were carried out using R Statistical Software 4.4.0 (R Core Team, 2013) and QGIS 3 (QGIS Development Team, 2020). We mainly used the r-packages raster (Hijmans et al., 2013), vegan (Oksanen et al., 2013), autopls (Schmidtlein et al., 2015), and rgdal (Bivand et al., 2015).

3.1. Sampling

A total of 153 sampling circles were selected and evenly distributed over each study area, with a diameter of 100 m and a step size of 300 m (Fig. 1). The diameter of 100 m was designed to ensure that the sample is large enough to cover material mixtures and to be covered by several spaceborne HSI pixels. The step size of 300 m was used to reduce the effects of spatial autocorrelation in the data (Griffith, 2005; Wang et al., 2012; Jilge et al., 2019). Consequently, the samples fully cover the diverse urban structures dominating the study site. In addition, each sample was numbered to enable better analysis and discussion later. Table 1 presents the material statistics of the samples in the two study areas.

3.2. Approach-OstOst

Approach-OstOst applies a gradient analysis following Jilge et al. (2019) to analyse the Ost area (Fig. 2), i.e., the samples collected in the Ost area generated the local urban material gradients using ordination methods and then form the Ost ordination space. Principal component analysis (PCA) was chosen as the ordination method in this study because it achieves the reduction by linear transformation of the data into principal components (PCs, treated as gradients given their physical meaning) and thus allows better comparability of different urban gradients. The first two PCs were selected according to the broken-stick model (Frontier, 1976; Jackson, 1993) in this study. A detailed discussion on the selection of the PCs in the transferability analysis of gradient and the determination of the number of PCs is found in Ji et al. (2020). Partial least square regression (PLSR) was used to regress the ordination scores of the

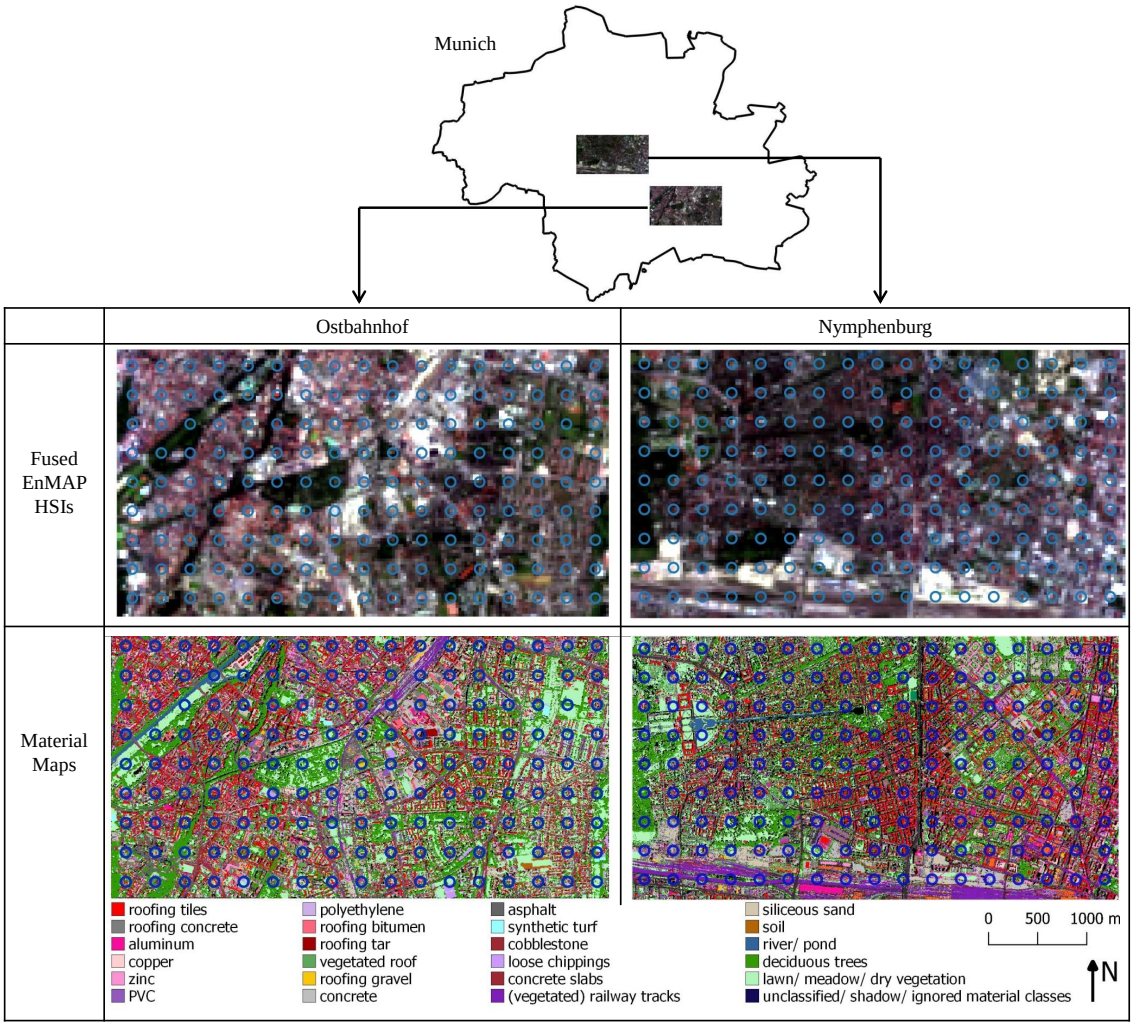

Figure 1: Two study areas: the Ostbahnhof (Ost) area and the Nymphenburg (Nym) area. The simulated HSIs are shown in true colour. The material maps include 27 valid material classes shown in their respective colours and unclassified/shadow/ignored material classes shown in black. The circles show the location and size of the collected samples.

samples against their reflectance values retrieved from Ost HSI to train the OstOst PLSR model. Finally, the PLSR model was applied on the Ost HSI to generate the OstOst prediction maps.

Approach-OstOst is a control approach and is expected to produce the most accurate prediction map. In this approach, both samples and ordination space were obtained from the Ost study area, leading to optimized model calibration. This approach serves as a reference in this study and therefore is used to evaluate the other approaches.

3.3. Approach-OstNym

Approach-OstNym deals with the situation in which the Ost area provides some samples but the number of these samples is insufficient to perform an urban material gradient analysis, while the samples collected in the Nym area allow a gradient analysis to be performed. In this case, the Ost samples were projected to the Nym ordination space and thus acquired their ordination scores in this ordination space (Fig. 2). The OstNym PLSR model was trained by PLS regressing the new ordination scores of the Ost samples against the reflectance values of samples. The prediction maps were obtained by applying the OstNym PLSR model on Ost HSI and are referred to as OstNym prediction maps.

Table 1: Statistics of the material map and sampling coverage in the Ost and Nym areas. The abbreviation of materials, total number of pixels for each material class and its proportion in the material map, and sampling coverage pixels for each material class and its proportion in total pixels per class.

Surface Material		Ost area				Nym area			
	Abbreviation	Total Pixels	class pixels/ total valid pixels (%)	Sampling Coverage	pixels in samples/ total valid pixels per class(%)	Total Pixels	class pixels/ total valid pixels (%)	Sampling Coverage	pixels in samples/ total valid pixels per class(%)
roofing tiles	rtil	66886	8.494	6138	9.177	74176	10.371	6929	9.341
roofing concrete	rcon	27440	3.485	2021	7.365	32908	4.601	2802	8.515
aluminum	ralu	10466	1.329	890	8.504	19538	2.732	2002	10.247
copper	rcop	13366	1.697	1149	8.596	6942	0.971	790	11.380
zinc	rzin	7607	0.966	611	8.032	10589	1.481	881	8.320
PVC	rpvc	13434	1.706	1107	8.240	12148	1.699	844	6.948
polyethylene	rpol	8625	1.095	793	9.194	5882	0.822	263	4.471
roofing bitumen	rbit	14883	1.890	1229	8.258	17931	2.507	1186	6.614
roofing tar	rtar	29249	3.715	2585	8.838	7236	1.012	569	7.863
vegetation roof	rveg	18879	2.398	1516	8.030	91709	12.823	7715	8.412
roofing gravel	rgra	8206	1.042	910	11.089	5176	0.724	398	7.689
concrete	fcon	42104	5.347	4275	10.153	37165	5.197	3065	8.247
asphalt	fasp	84854	10.776	6915	8.149	67080	9.379	6082	9.067
synthetic turf	fkun	3209	0.408	291	9.068	675	0.094	32	4.741
cobblestone	pcob	47358	6.014	4046	8.543	37754	5.279	3111	8.240
loose chippings	prlc	20546	2.609	2199	10.703	6733	0.941	588	8.733
concrete slabs	pcon	11015	1.399	954	8.661	1578	0.221	120	7.605
railway tracks	prail	10811	1.373	780	7.215	55175	7.715	4179	7.574
vegetated railway tracks	prailveg	11546	1.466	937	8.115	2280	0.319	123	5.395
siliceous sand	bsan	11765	1.494	1050	8.925	14558	2.036	1550	10.647
humous soil	bsoi	2978	0.378	180	6.044	1528	0.214	95	6.217
river	wriv	4518	0.574	484	10.713	2518	0.352	224	8.896
pond	wpon	4691	0.596	401	8.548	430	0.060	5	1.163
deciduous trees	vdec	172784	21.943	14053	8.133	115810	16.193	9682	8.360
lawn	vlaw	16983	2.157	1471	8.662	37133	5.192	3632	9.781
meadow	vmea	87525	11.115	7774	8.882	43176	6.037	3578	8.287
dry vegetation	vdry	35690	4.533	3165	8.868	7364	1.030	687	9.329
Total Valid Pixels		787418	100			715192	100		
Deleted Pixels		75994				148220			
Total Pixels		863412				863412			

3.4. Approach-NymNym

Approach-NymNym deals with the situation in which no Ost samples could be collected, and thus, information from the Nym area was used to interpret the Ost area. In this approach, the ordination scores of the Nym samples in Nym ordination space were PLS-regressed against their reflectance values to generate a NymNym PLSR model (Fig. 2). Applying this PLSR model on Ost HSI, the Ost area was interpreted without in situ information.

3.5. Comparison of approaches

The three approaches were compared based on the intermediate results obtained from each step. First, the sample distributions in the two ordination spaces were compared visually and statistically using the Mantel test (Peres-Neto and Jackson, 2001) to acquire an overall estimate of whether the sample distributions in the two ordination spaces match. The Mantel test was based on a Pearson correlation in this study between two dissimilarity matrices of the samples' material tables. The Mantel test adopts a permutation test with randomly permuting rows and columns of the dissimilarity matrix of samples' scores on two PCs 999 times (Legendre and Legendre, 2012) and then recalculates the correlation after each permutation to assess the significance of the observed correlation which is the proportion of permutations that lead to a higher correlation coefficient. In addition to overcoming the problems arising from the statistical dependence of the elements within each of the two matrices, the use of the permutation test means that there is no reliance on assumptions about the statistical distributions of the elements in the matrices.

PLSR models were subsequently generated from the ordination scores of the samples and the sample-averaged reflectance values. It should be noted that the OstNym and NymNym PLSR models were based on the

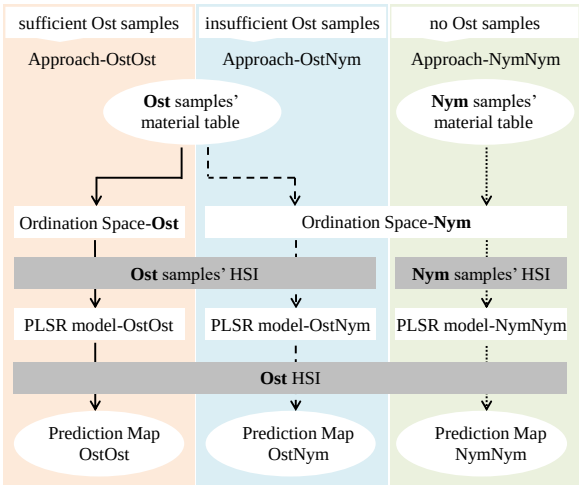

Figure 2: Study workflow: overview of three approaches. Three approaches are proposed to deal with different situations: sufficient, insufficient, and no Ost samples. Ost samples are used in approach-OstOst and approach-OstNym to produce the PLSR models, while Nym samples are used in approach-NymNym. Ost ordination space is used in approach-OstOst, while Nym ordination space is used in approach-OstNym and approach-NymNym.

same ordination space—Nym ordination space—with a corresponding set of samples (Ost samples and Nym samples).

Third, the resulting prediction maps obtained from three approaches were visually assessed. When applying the PLSR models to the Ost HSI, three groups of prediction maps were obtained from the three approaches.

In the last step, four groups of samples were selected to demonstrate that a closer location in the ordination space corresponds to more similar material compositions. In addition, the reflectance values were also compared to prove the difference between reflectance values of the Ost area and the Nym area and to prove that the NymNym PLSR model can be applied on the Ost area.

4. Results

4.1. Ordination spaces

The Ost ordination space and Nym ordination space are shown in Fig. 3. Fig. 3a presents the ordination space generated from Ost samples that is used for approach-OstOst. Fig. 3b shows the ordination space generated from Nym samples that is used in approach-OstNym and approach-NymNym with the assumption that insufficient or no Ost samples generate the ordination space. All of the samples are projected into both ordination spaces, with material vectors representing the directions of increase in the respective material cover fractions.

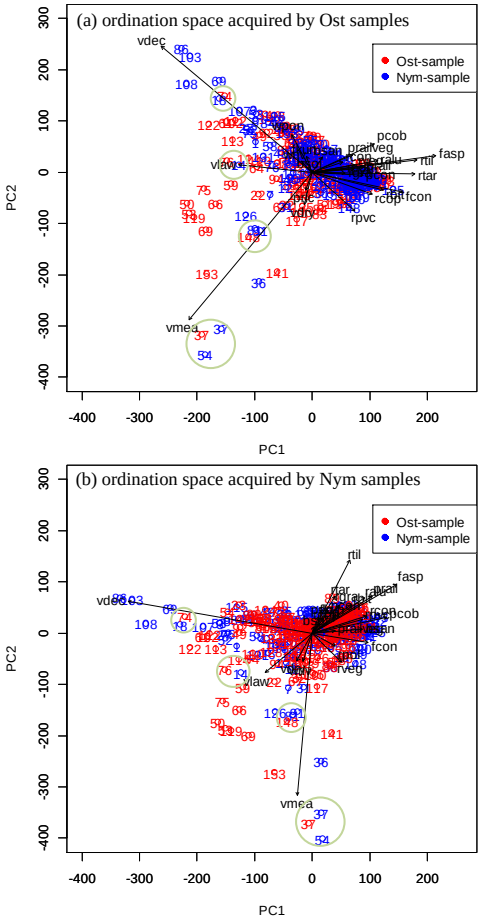

Figure 3: Ordination spaces generated from the samples of the Ost and Nym areas. (a) is used in approach-OstOst, and (b) is used in approach-OstNym and approach-NymNym. Ost and Nym samples are presented, and the potential material vector and their length are also given. The full names of the materials are given in Table 1. In addition, the green circles highlight four groups of samples with closely spaced positions.

The distributions of the samples between Ost ordination space and Nym ordination space are similar. Generally, both sample cloud distributions have a triangular shape. A detailed examination shows that most representative material classes are similar. For example, most vegetation types, such as deciduous trees(*vdec*), meadow(*vmea*), and lawn(*vlaw*) are on one side and other materials (mostly artificial materials) on the other. The vector length of vegetation types are longer because they cover more pixels. Furthermore, the distances between the samples are relatively constant. For example, the distances are consistent within the group of Nym-sample-86, Nym-sample-103 and Nym-sample-108, as

well as for the group of Ost-sample-37, Nym-sample-37, and Nym-sample-54.

Mantel statistics also show the consistent configuration of the distribution of the samples in two ordination spaces. The Mantel statistical result of the Ost samples is 0.995 with a significance of 0.001 in 999 free permutations, while that of the Nym samples is 0.990, with a significance of 0.001 in 999 free permutations.

4.2. PLSR models

We generated six PLSR models by regressing the ordination scores in each gradient and the samples' averaged reflectance values. The best PLSR model for PC1 resulted in R^2= 0.898 for calibration and R^2= 0.892 in 10-fold cross-validation (Fig. 4a). Accordingly, the PLSR models of PC1 from approach-OstNym and approach-NymNym also acquire relatively high R^2 (0.760, 0.743; 0.860; 0.836) (Fig. 4b, 4c). For the PC2, the PLSR models resulted in R^2= 0.433 for calibration and R^2= 0.351 (Fig. 4d) in 10-fold cross-validation for approach-OstOst, and for approach-OstNym and approach-NymNym are 0.698, 0.648, 0.736, and 0.646 (Fig. 4e, 4f).

The distribution of samples in Fig. 4 corresponds to the distribution of samples in Fig. 3. The approach-OstOst evaluates the ordination scores in the Ost ordination space, and therefore, the distribution of the samples in PC1 is dense and ranges from -200 to 200 in PC2. The approach-OstNym and approach-NymNym apply the ordination scores of the Nym ordination space, and therefore, the distribution in PC1 is loose and ranges from -200 to 100 in PC2.

For approach-OstOst, PC1 (Fig. 4a) contains the largest variance, and PC2 (Fig. 4d) represents less information and consequently shows a relation to the reflectance values modelled with relatively low R^2. The approach-OstNym and approach-NymNym acquired reasonable PLSR models and performed well with 10-fold cross validation, indicating that the reflectance values of the Ost samples and their ordination scores in the Nym ordination space can reasonably build a PLSR model. In particular, the higher values of calibration and validation of PC2 in approach-OstNym (Fig. 4e) indicate that the PC2 in approach-OstNym provides more accurate information than the PC2 in approach-OstOst. Similarly, the relatively high value of calculation R^2 and validation R^2 of the PLSR models of two PCs in approach-NymNym prove that the ordination scores of the Nym samples in Nym ordination space and their reflectance values established an accurate PLSR model.

4.3. Prediction maps

Prediction maps were acquired by applying the corresponding PLSR models to the Ost HSI. The prediction map obtained from the PC1 PLSR model of approach-OstOst (Fig. 5a) presents the pattern of vegetation in blue and artificial materials in red, and the PC2 prediction map (Fig. 5d) presents the different vegetation species with rather low accuracy. The prediction maps generated from approach-OstNym provide similar information: the resulting PC1 prediction map (Fig. 5b) vividly displays vegetation coverage, and the structures of artificial materials are similarly indicated; the PC2 prediction map (Fig. 5e) also shows the vegetation information. While the prediction maps produced from approach-NymNym appear to lose some detailed information, the major features are provided: the PC1 prediction map (Fig. 5c) presents the information of vegetation and artificial materials, while the PC2 prediction map (Fig. 5f) shows the vegetation coverage of the study area.

Two interesting phenomena are observed in the prediction maps. The trapezoidal area (A) in Fig. 5a, called the Ostfriedhof area, shows variable intensity of the blue colour. The left side is light blue, and the right side is dark blue. In the historical image review by Google at the time closest to the acquisition time of the HyMap data, the area was divided into two subareas, with the left side including more graves, i.e., more impervious surfaces, while the right side containing less graves. The trapezoidal area (B) (Fig. 5b) shows two types of patterns with red on the left and blue on the right. Google Earth historical imagery check reveals that the left block contained row houses and the right block contained semi-detached houses. The semi-detached houses had much more vegetation than the row houses and are therefore coloured blue, while the the row houses block is coloured red in the prediction map.

4.4. Comparison of material compositions and reflectance values of sample groups

Four groups of samples were selected in the ordination spaces within green circles (Fig. 3) for which the reflectance values and material compositions are provided in Fig. 6. The first group includes Ost-sample-74 and Nym-sample-18 that have similar material compositions. Since lawn (vlaw) and meadow (vmea) have similar reflectance values, the difference between these two samples is that Ost-sample-74 covers a small amount of asphalt (fasp). Given that the vegetation species have stronger spectral features, their reflectance should not vary much. However, their reflectance values do vary considerably (Fig. 6a). The

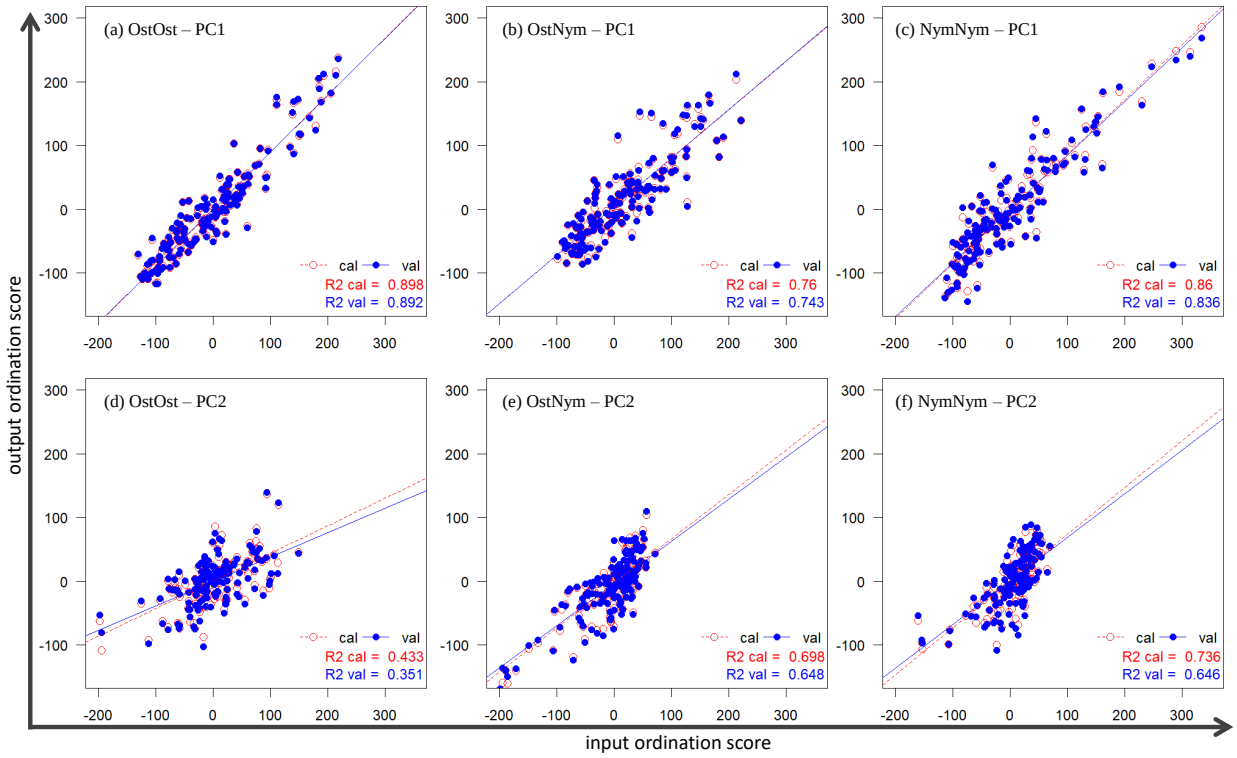

Figure 4: The performance of PLSR models in three approaches. R^2 cal: R^2 in calibration, R^2 val: R^2 in 10-fold validation. Each approach has two PLSR models of PC1-reflectance and PC2-reflectance. Circles or points represent samples. The x-axis represents the input ordination scores of the samples used to build the PLSR model, and the y-axis represents the output ordination scores, while the calculated scores of the PLSR model are represented by red circles and the predicted scores of the 10-fold cross-validation of the PLSR model are represented by blue points. Their fit lines and R^2 are provided and displayed in corresponding colours. $y = x$ represented the best possible fit with either calculated or validated ordination scores of the samples matching the input ordination scores and therefore the best possible calculation or validation R^2 is 1.

Ost-sample-76 and Nym-sample-14 in the second group are distantly close in the ordination space, and have similar material and same reflectance values, which fits very well with the application of transferable urban material gradients. The other two groups comprise three samples, and show the difference between the reflectance values of Ost and Nym HSIs. Fig. 6c displays the material portions and reflectance of Ost-sample-148, Nym-sample-81, and Nym-sample-91. Nym-sample-81 and Nym-sample-91 are closer in the ordination space (Fig. 3), and have similar materials (meadow, deciduous trees, roofing vegetation, and cobblestone) with similar proportions, and this is reflected in their spectra. The last group includes Ost-sample-37, Nym-sample-37, and Nym-sample-54 (Fig. 6d). The Ost-sample-37 is located in the middle of two Nym samples, but the reflectance values of Ost-sample-37 are the lowest, and the other spectra of the Nym samples are characterized to be more similar. While Fig. 6b and 6c demonstrate the similarity of the reflectance values of the Ost and Nym areas, Fig. 6a and 6d show the differences between the reflectance values of these two areas.

5. Discussion

5.1. Are the urban material gradients transferable between two study sites?

Theoretically, the transferability of urban material gradients means that the gradients acquired from one area are suitable for the interpretation of another area, i.e., the approach-OstNym, using Nym gradients to interpret Ost area, performs as well as approach-OstOst. The difference between these two approaches is the gradients, i.e. approach-OstOst uses the Ost gradients and approach-OstNym uses the Nym gradients. Other factors, such as the material composition of the samples and their reflectance values, are fully controlled because the samples used are always Ost samples. As shown in section 4, for the sample distribution in the ordination spaces, the performance of PLSR models, and the

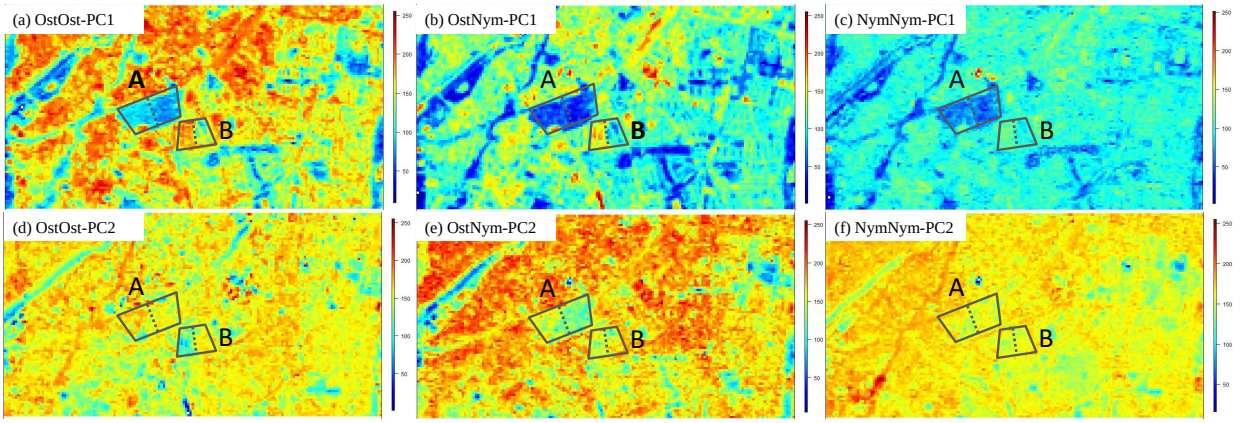

Figure 5: Prediction maps for each PC. Subfigures (a) - (f) show the prediction maps for each PC obtained directly from the PLSR models. For better visual interpretation, PC1 is inverted so that the vegetation pattern is shown in blue and artificial materials in red. On the one hand, three pairs of prediction maps show similar patterns including vegetation coverage and urban structures. On the other hand, detailed information is gradually lost from the prediction maps of approach-OstOst, approach-OstNym, and approach-NymNym.

prediction maps, the approach-OstOst and approach-OstNym exhibit very similar results. Therefore, the urban material gradients are transferable between the Ost and Nym areas.

This means that the material gradients acquired from the Nym area can be used to successfully interpret the Ost area. This is investigated by approach-NymNym and demonstrated the quality of the results through the comparison of approach-OstOst and approach-NymNym. The intermediate results indicate that their ordination spaces are similar and PLSR models performs quite well. However, although the prediction maps of the approach-NymNym retain the main characteristics of the Ost area, they still loses some detailed information.

The comparison of approach-OstOst and approach-NymNym shows that the good performance of the PLSR models does not always mean that both approaches can achieve good interpretation results on the Ost area. The OstOst PLSR model is based on the ordination scores of the Ost samples and reflectance values of the Ost area, whereas the NymNym PLSR model describes the relation between the ordination scores of the Nym samples and the Nym reflectance values. In both ordination spaces (Fig. 3), the samples in close proximity to each other have similar material compositions, and thus we can assume that either the Ost sample or the Nym sample can be treated as equivalent. In another words, the samples in close proximity in the ordination space should have qualitatively similar reflectance values. If this is in fact the case, approach-NymNym should display similar information to that obtained by approach-OstOst, i.e. the urban material gradients are transferable under application from the Nym area to the Ost area.

To determine whether the reflectance values vary between Ost and Nym HSIs, four groups of samples were selected in the ordination spaces within the green circles (Fig. 3) for which the reflectance values and material compositions are provided in Fig. 6. The second and third groups of the samples show the consistent reflectance values between the Ost and Nym samples, while the first and last groups demonstrate that some samples from the Ost and Nym areas do not show consistent reflectance values. Therefore, the PLSR models acquired in approach-NymNym cannot be simply applied to interpret the Ost area, as they are calculated for Nym HSIs, and there is a difference between the reflectance of Ost and Nym HSIs. This phenomenon is discussed further in the next section.

5.2. *What affects the transferability of urban material gradients?*

The gradient concept is based on the assumption that similar material compositions in the gradient space result in similar spectral reflectance mixture characteristics. Therefore, the consistency of reflectance values from HSIs between the areas are relevant as mentioned above. The neighboring samples in the ordination space (Fig. 3a) have similar material composition, and therefore, the difference between the resulting OstNym and NymNym prediction maps shown in Fig. 3a is related to the difference of the reflectance values between the Ost and Nym areas. A possible reason for this observation is the underlying data source for the simulated

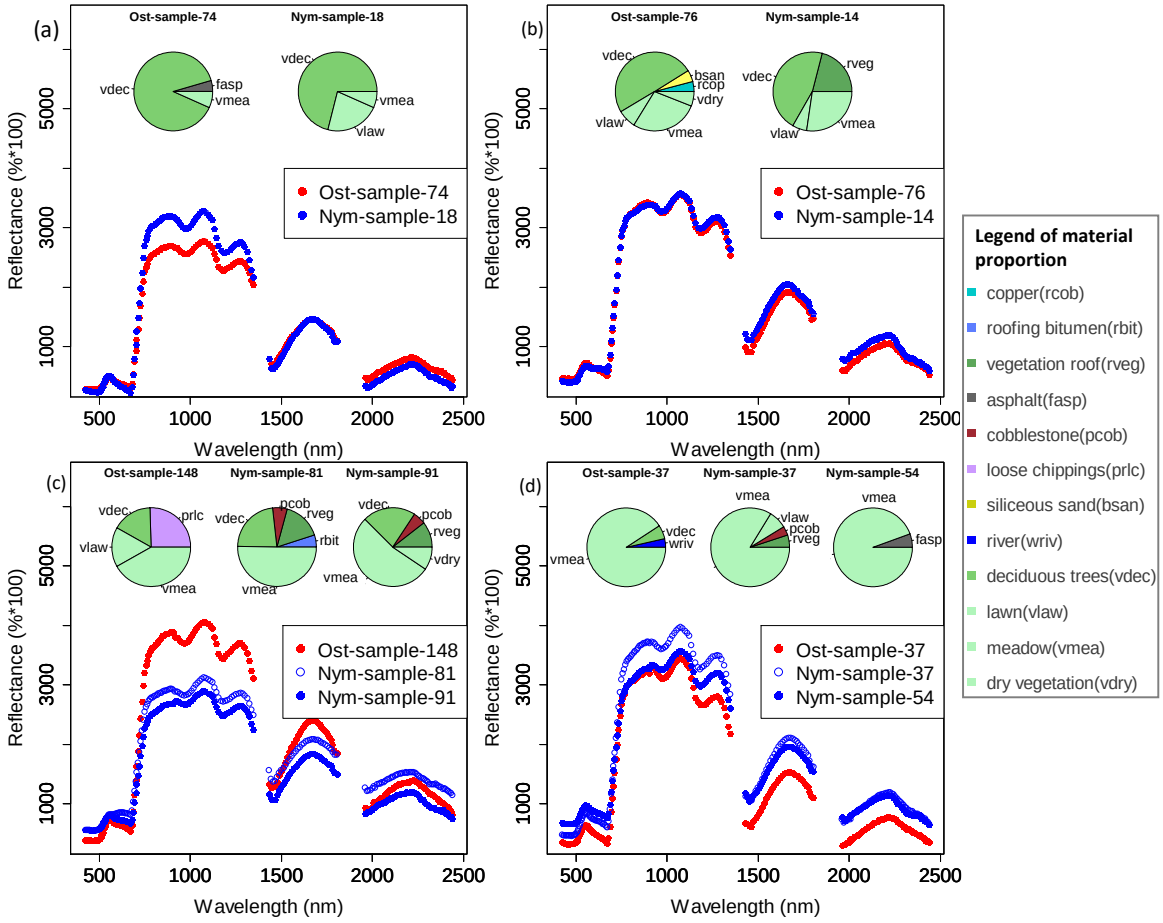

Figure 6: Comparison of reflectance values. Four sets of samples are selected from the ordination space (refer to Fig. 3 for detailed discussion. The material compositions of the samples are provided. The material covering less than 15 pixels are neglected in this figure that represents approximately 3% of the total covering pixels of a sample. The color of the material is consistent with Fig. 1.

EnMAP data as described in Section 2.2. Several airborne HyMap flight lines are combined to generate the EnMAP simulated data set. These flight lines show that differences in the brightness level that still remain can be traced back to the remaining BRDF effects that are then also present in the simulated EnMAP data. It can be expected that real spaceborne HSI data will not show these local brightness differences. However, for this study, real spaceborne HSI data that matches the used surface material map of Munich were not available. Future studies with real spaceborne HSI information such as that from PRISMA or DESIS data are expected to obtain prediction maps with higher accuracy.

Another aspect that affect the transferability of urban material gradients is the material composition of the two areas. Since the PLSR model is trained with a specific set of materials of the first area, new materials in the second area cannot be considered in the PSLR model and therefore, will most likely result in lower model performance. In other words, the new material in the unknown area will not be recognized due to the lack of appropriate input in the training of the PLSR model. Therefore, the detected materials from the gradients acquired in the known area are detectable in the unknown area. In the case of the Ost and Nym areas, we can expect almost the same material composition. This should be also the case for different cities in Germany that consist of similar urban neighborhoods. Future studies shall be dedicated to test the transferability of gradients from one city to a similar but different city. To build a more robust model for several cities, gradients can also be derived from test areas of different cities with varying surface material compositions.

Although the results confirm that urban material gradients are transferable between two study sites, the physical significance of the gradients produced by PCA

changed slightly between the Ost to Nym ordination spaces. In the Ost ordination space, the negative end of PC1 represents vegetation classes (including deciduous tree, lawn, and meadow), and the positive end of PC1 represents an abundance of artificial materials (e.g., cobblestone, asphalt, roofing tar, and concrete). Thus, the negative end of PC2 can be used to discriminate deciduous trees and meadow. In the Nym ordination space, PC1 can still differentiate the vegetation species and artificial materials but in a less distinctive manner; e.g., meadow is not clearly separated by PC1 any more. In addition, PC2 cannot be used to quantitatively distinguish deciduous trees and lawn. However, it should be noted here that PCA is not the optimal method for the interpretation of physical significance of urban gradients (see Ji et al., 2020) but rather is designed to test the transferability that was the main objective of this paper. Therefore, we suggest that other ordination methods should be used to obtain the most meaningful urban gradients such as shown in Jilge et al. (2019). However, PCA is still considered as one of the most appropriate methods for the transferablity analysis of urban gradients across different areas because it can easily transfer gradients with loadings between different study areas. Moreover, the resulting urban material gradients obtained from different ordination methods usually have similar properties. Thus, since we demonstrate the transferability of the gradients determined by PCA, the gradients determined by other ordination methods are transferable in the same situation.

The prediction maps are comparable to those acquired by Jilge et al. (2019). Although Jilge et al. (2019) applied detrended correspondence analysis (DCA), the prediction maps obtained in their study contain similar information to that obtained in this work, in particular for PC1. Considering these results together with the above discussion suggests that ordination methods can affect the prediction results, but will not change them completely. Skowronek et al. (2018) et al. evaluated the transferability of HSI-based distribution models for the detection of an invasive alien bryophyte. Skowronek et al. (2018) concluded that the success of transfer models calibrated in one site to another site depend strongly on the respective study sites. Two or more ordination methods are suggested to be used in parallel to enhance the detection of artefacts in the results, because each ordination methods with the different weightings of the elements in the species abundance matrix, and thus may explain the observed variation in the analysed ordination results. It will be interesting to examine these approaches in future studies in order to enhance our understanding of the functionality, robustness and feasibility of the methods for deriving urban gradients.

5.3. Potential applications of transferable urban gradients

Transferable urban material gradients can be used for time- and cost-efficient large-scale mapping of urban materials. The potential use of remote sensing images for urban mapping has studied extensively over the past decade (Ridd, 1995; Weng, 2012). Since spaceborne HSIs cover large geographical areas in high geometric detail and with a short revisiting time, their capabilities were demonstrated. However, some of the urgently needed detailed information cannot be obtained from HSIs and must be derived from other sources. To create classification maps that are useful for urban planners, supervised classification methods are commonly implemented on HSIs. These rules lead to results with an accuracy that is strongly influenced by the amount of training data. Obtaining appropriate ground truth data for implementation and validation purposes requires intense efforts in terms of time consumption and economic resources. For most areas, in situ data are either completely absent or are outdated and unreliable. Therefore, the limited availability of in situ data is a challenge for classification problems, particularly with regard to the model transferability. The transferred urban gradients provides a possible approach for avoiding training data collection in the area that has an known area in close proximity and fits the transferable urban gradients.

Transferable urban gradients provide a practical method to obtain a fuzzy map of an unknown area with limited information and therefore can be used to improve the results of other urban mapping models. First, the transfer of urban gradients can be an useful approach for mapping urban materials when limited resources are available to carry out fieldwork and remote sensing data are available for a larger area. With a limited training set, classification accuracy tends to decrease as the number of features increases which is known as the Hughes effect (Hughes, 1968). As an increasing number of mathematical or machine learning methods are proposed with the requirement of sufficient prior knowledge, transferable urban material gradients can provide more knowledge-based information for use in these algorithms. The prior knowledge including spatial relationships and patterns of urban structures can be used to improve the characterization of not only single pixels but also of the whole image (Plaza et al., 2009).

6. Conclusion

Gradient analysis has the potential to be applicable to images from the ongoing and future spaceborne imaging spectroscopy missions. Although the spatial resolution of these data is considered to be coarse for urban applications and urban object-related information cannot be directly detected, it enables the derivation of surface material compositions of large areas, which is important information for continental to global urban climate related analyses.

In this paper, we addressed the question of whether gradient analysis can be a robust and transferable technique despite its data-driven nature. For this purpose, we designed three tests for simulating the transferability of urban material gradients to the Ostbahnhof area in Munich, Germany.

In the first step, we evaluated the similarity of the sample distributions in two ordination spaces, one built by the samples of the Ostbahnhof area and the other generated by the samples of the Nymphenburg area. Both gradient spaces are highly comparable, providing an initial indication of the robustness of the urban gradients in the case where the overall surface material composition is similar. It can be assumed that these gradients are applicable to other cities with similar urban structures and thus surface material compositions, so that this method will be valid for a wide range of mid-European cities. However, if new and region-specific materials are dominating the surface material composition such as for cities with other urban structures, the gradients may differ.

We expanded the transferability test to regress the gradient scores against the surface material reflectances using PLSR and applied the resulting models to predict the surface material compositions of Ostbahnhof area using imaging spectroscopy data. The comparison of the prediction results of approach-OstOst and approach-OstNym demonstrates that the material gradients acquired from the Nym area can successfully interpret the Ost area, while the comparison of approach-OstOst and approach-NymNym show that the PLSR model retrieved from Nym area cannot be simply transferred to the Ost area.

Since this contradicts the results of the gradient space analyses, we found that the reflectance data of the two investigated areas have significant differences in the albedo despite their similar surface material compositions. This can be related to the different flight lines of the source airborne data from HyMap used for the simulation of spaceborne EnMAP data. Although we cannot fully prove the transferability of the PLSR models to different areas, the results indicate the transferability potential if well-calibrated spaceborne imaging spectroscopy data are used. Moreover, these results reveal the importance of calibrated spaceborne imaging spectroscopy data and data cross-calibration, if different spaceborne sensor data are combined.

Transferable urban material gradients can be used effectively in time-consuming and costly large-scale mapping of urban material compositions. Furthermore, they can provide a fuzzy map of an unknown area with limited information and therefore can be used to enhance the results of other urban mapping models. Although the gradient concept works well in ecology for mixed vegetation, the ability of this approach should be further tested in the field of urban material composition. Exploration of urban material gradients, focusing not only on its transferability but also on pattern recognition capability, will provide us with a more accurate and definite answer to this question.

7. Acknowledgements

This work was supported by the China Scholarship Council under scholarship No. 201806220088. We would like to thank Dr. Wieke Heldens and Dr. Marianne Jilge from the German Aerospace Center (DLR) for providing and pre-processing the surface material map of Munich.

References

Alonso, K., Bachmann, M., Burch, K., Carmona, E., Cerra, D., de los Reyes, R., Dietrich, D., Heiden, U., Hölderlin, A., Ickes, J., Knodt, U., Krutz, D., Lester, H., Müller, R., Pagnutti, M., Reinartz, P., Richter, R., Ryan, R., Sebastian, I., Tegler, M., 2019. Data Products, Quality and Validation of the DLR Earth Sensing Imaging Spectrometer (DESIS). Sensors 19, 4471. doi:10.3390/s19204471.

Auer Jr, A.H., 1978. Correlation of land use and cover with meteorological anomalies. Journal of Applied Meteorology 17, 636–643.

Bivand, R., Keitt, T., Rowlingson, B., Pebesma, E., Sumner, M., Hijmans, R., Rouault, E., Bivand, M.R., 2015. Package 'rgdal'. Bindings for the Geospatial Data Abstraction Library. Available online: https://cran. r-project. org/web/packages/rgdal/index. html (accessed on 15 October 2017) .

Cao, W., Dong, L., Wu, L., Liu, Y., 2020. Quantifying urban areas with multi-source data based on percolation theory. Remote Sensing of Environment 241, 111730.

Chen, F., Jiang, H., Van de Voorde, T., Lu, S., Xu, W., Zhou, Y., 2018. Land cover mapping in urban environments using hyperspectral APEX data: A study case in Baden, Switzerland. International Journal of Applied Earth Observation and Geoinformation 71, 70–82.

Degerickx, J., Roberts, D.A., McFadden, J.P., Hermy, M., Somers, B., 2018. Urban tree health assessment using airborne hyperspectral and LiDAR imagery. International Journal of Applied Earth Observation and Geoinformation 73, 26–38.

DESA, U., 2018. 2018 revision of world urbanization prospects.

Feilhauer, H., Dahlke, C., Doktor, D., Lausch, A., Schmidtlein, S., Schulz, G., Stenzel, S., 2014. Mapping the local variability of Natura 2000 habitats with remote sensing. Applied Vegetation Science 17, 765–779.

Feilhauer, H., Faude, U., Schmidtlein, S., 2011. Combining Isomap ordination and imaging spectroscopy to map continuous floristic gradients in a heterogeneous landscape. Remote Sensing of Environment 115, 2513–2524.

Feilhauer, H., Zlinszky, A., Kania, A., Foody, G.M., Doktor, D., Lausch, A., Schmidtlein, S., 2020. Let your maps be fuzzy!—class probabilities and floristic gradients as alternatives to crisp mapping for remote sensing of vegetation. Remote Sensing in Ecology and Conservation .

Frontier, S., 1976. Decrease of eigenvalues in principal component analysis-comparison with broken stick model. Journal of Experimental Marine Biology and Ecology 25, 67–75.

Griffith, D.A., 2005. Effective geographic sample size in the presence of spatial autocorrelation. Annals of the Association of American Geographers 95, 740–760.

Guanter, L., Kaufmann, H., Segl, K., Foerster, S., Rogass, C., Chabrillat, S., Kuester, T., Hollstein, A., Rossner, G., Chlebek, C., Straif, C., Fischer, S., Schrader, S., Storch, T., Heiden, U., Mueller, A., Bachmann, M., Mühle, H., Müller, R., Habermeyer, M., Ohndorf, A., Hill, J., Buddenbaum, H., Hostert, P., Van der Linden, S., Leitão, P.J., Rabe, A., Doerffer, R., Krasemann, H., Xi, H., Mauser, W., Hank, T., Locherer, M., Rast, M., Staenz, K., Sang, B., 2015. The EnMAP Spaceborne Imaging Spectroscopy Mission for Earth Observation. Remote Sensing 7, 8830–8857. Number: 7 Publisher: Multidisciplinary Digital Publishing Institute.

Heiden, U., Heldens, W., Roessner, S., Segl, K., Esch, T., Mueller, A., 2012. Urban structure type characterization using hyperspectral remote sensing and height information. Landscape and Urban Planning 105, 361–375.

Heiden, U., Segl, K., Roessner, S., Kaufmann, H., 2007. Determination of robust spectral features for identification of urban surface materials in hyperspectral remote sensing data. Remote Sensing of Environment 111, 537–552.

Heldens, W., 2010. Use of airborne hyperspectral data and height information to support urban micro climate characterisation. Ph.D. thesis. University Wuerzburg. Germany.

Herold, M., Roberts, D., Gardner, M., Dennison, P., 2004. Spectrometry for urban area remote sensing—development and analysis of a spectral library from 350 to 2400 nm. Remote Sensing of Environment 91, 304–319.

Hijmans, R.J., van Etten, J., Mattiuzzi, M., Sumner, M., Greenberg, J., Lamigueiro, O., Bevan, A., Racine, E., Shortridge, A., 2013. Raster package in r.

Hughes, G., 1968. On the mean accuracy of statistical pattern recognizers. IEEE Transactions on Information Theory 14, 55–63. Conference Name: IEEE Transactions on Information Theory.

Jackson, D.A., 1993. Stopping rules in principal components analysis: a comparison of heuristical and statistical approaches. Ecology 74.

Ji, C., Jilge, M., Heiden, U., Stellmes, M., Feilhauer, H., 2020. Sampling Robustness in Gradient Analysis of Urban Material Mixtures. IEEE Transactions on Geoscience and Remote Sensing , 1–11doi:10.1109/TGRS.2020.3040342. conference Name: IEEE Transactions on Geoscience and Remote Sensing.

Jilge, M., Heiden, U., Neumann, C., Feilhauer, H., 2019. Gradients in urban material composition: A new concept to map cities with spaceborne imaging spectroscopy data. Remote Sensing of Environment 223, 179–193.

Kruse, F., Boardman, J., Huntington, J., 2003. Comparison of airborne hyperspectral data and EO-1 Hyperion for mineral mapping. IEEE Transactions on Geoscience and Remote Sensing 41, 1388–1400.

Lakes, T., Kim, H.O., 2012. The urban environmental indicator "biotope area ratio"—an enhanced approach to assess and manage the urban ecosystem services using high resolution remote-sensing. Ecological Indicators 13, 93–103.

Lee, C.M., Cable, M.L., Hook, S.J., Green, R.O., Ustin, S.L., Mandl, D.J., Middleton, E.M., 2015. An introduction to the NASA Hyperspectral InfraRed Imager (HyspIRI) mission and preparatory activities. Remote Sensing of Environment 167, 6–19.

Legendre, P., Legendre, L., 2012. Numerical ecology. Elsevier.

Li, J., Bioucas-Dias, J.M., Plaza, A., 2012. Spectral–Spatial Hyperspectral Image Segmentation Using Subspace Multinomial Logistic Regression and Markov Random Fields. IEEE Transactions on Geoscience and Remote Sensing 50, 809–823. Conference Name: IEEE Transactions on Geoscience and Remote Sensing.

van der Linden, S., Okujeni, A., Canters, F., Degerickx, J., Heiden, U., Hostert, P., Priem, F., Somers, B., Thiel, F., 2019. Imaging Spectroscopy of Urban Environments. Surveys in Geophysics 40, 471–488.

Loizzo, R., Daraio, M., Guarini, R., Longo, F., Lorusso, R., Dini, L., Lopinto, E., 2019. Prisma Mission Status and Perspective, in: IGARSS 2019 - 2019 IEEE International Geoscience and Remote Sensing Symposium, pp. 4503–4506. doi:10.1109/IGARSS.2019.8899272. iSSN: 2153-7003.

Neumann, C., 2017. Spatial nature conservation monitoring on the basis of ecological gradients using imaging spectroscopy. Ph.D. thesis. Technischen University Berlin. Accepted: 2017-07-18T16:10:59Z.

Neumann, C., Förster, M., Kleinschmit, B., Itzerott, S., 2016. Utilizing a PLSR-Based Band-Selection Procedure for Spectral Feature Characterization of Floristic Gradients. IEEE Journal of Selected Topics in Applied Earth Observations and Remote Sensing 9, 3982–3996. Conference Name: IEEE Journal of Selected Topics in Applied Earth Observations and Remote Sensing.

Nieke, J., Rast, M., 2019. Status: Copernicus Hyperspectral Imaging Mission For The Environment (CHIME), in: IGARSS 2019 - 2019 IEEE International Geoscience and Remote Sensing Symposium, pp. 4609–4611. doi:10.1109/IGARSS.2019.8899807. iSSN: 2153-7003.

Oksanen, J., Blanchet, F.G., Kindt, R., Legendre, P., Minchin, P.R., O'hara, R., Simpson, G.L., Solymos, P., Stevens, M.H.H., Wagner, H., et al., 2013. Package 'vegan'. Community ecology package, version 2, 1–295.

Peres-Neto, P.R., Jackson, D.A., 2001. How well do multivariate data sets match? The advantages of a Procrustean superimposition approach over the Mantel test. Oecologia 129, 169–178.

Plaza, A., Benediktsson, J.A., Boardman, J.W., Brazile, J., Bruzzone, L., Camps-Valls, G., Chanussot, J., Fauvel, M., Gamba, P., Gualtieri, A., Marconcini, M., Tilton, J.C., Trianni, G., 2009. Recent advances in techniques for hyperspectral image processing. Remote Sensing of Environment 113, S110–S122.

QGIS Development Team, 2020. QGIS Geographic Information System. Open Source Geospatial Foundation Project.

R Core Team, 2013. R: A Language and Environment for Statistical Computing. R Foundation for Statistical Computing. Vienna, Austria. URL: `http://www.R-project.org/`.

Ridd, M.K., 1995. Exploring a vis (vegetation-impervious surface-soil) model for urban ecosystem analysis through remote sensing: comparative anatomy for cities. International journal of remote sensing 16, 2165–2185.

Schmidtlein, S., Oldenburg, C., Feilhauer, H., Mevik, B.H., 2015. Package 'autopls'. Partial least square regression with backward selection of predictors.[WWW Document]. URL https://cran. r-project. org/web/packages/autopls/index. html (accessed 7.1. 17) .

Schmidtlein, S., Sassin, J., 2004. Mapping of continuous floristic gradients in grasslands using hyperspectral imagery. Remote Sensing

of Environment 92, 126–138.

Segl, K., Guanter, L., Rogass, C., Kuester, T., Roessner, S., Kaufmann, H., Sang, B., Mogulsky, V., Hofer, S., 2012. EeteS—The EnMAP End-to-End Simulation Tool. IEEE Journal of Selected Topics in Applied Earth Observations and Remote Sensing 5, 522–530.

Seto, K.C., Shepherd, J.M., 2009. Global urban land-use trends and climate impacts. Current Opinion in Environmental Sustainability 1, 89–95.

Skowronek, S., Van De Kerchove, R., Rombouts, B., Aerts, R., Ewald, M., Warrie, J., Schiefer, F., Garzon-Lopez, C., Hattab, T., Honnay, O., Lenoir, J., Rocchini, D., Schmidtlein, S., Somers, B., Feilhauer, H., 2018. Transferability of species distribution models for the detection of an invasive alien bryophyte using imaging spectroscopy data. International Journal of Applied Earth Observation and Geoinformation 68, 61–72.

Wang, J.F., Stein, A., Gao, B.B., Ge, Y., 2012. A review of spatial sampling. Spatial Statistics 2, 1–14.

Weng, Q., 2012. Remote sensing of impervious surfaces in the urban areas: Requirements, methods, and trends. Remote Sensing of Environment 117, 34–49.